[CANCER RESEARCH 64, 4270–4276, June 15, 2004]

Molecular Causes of the Aberrant Choline Phospholipid Metabolism in Breast Cancer

Kristine Glunde,[1] Chunfa Jie,[2] and Zaver M. Bhujwalla[1]

[1]Magnetic Resonance Oncology Section, Division of Magnetic Resonance Research, Department of Radiology and [2]Institute of Genetic Medicine, Johns Hopkins University School of Medicine, Baltimore, Maryland

ABSTRACT

Proton magnetic resonance spectroscopy (^{1}H MRS) consistently detects significant differences in choline phospholipid metabolites of malignant *versus* benign breast lesions. It is critically important to understand the molecular causes underlying these metabolic differences, because this may identify novel targets for attack in cancer cells. In this study, differences in choline membrane metabolism were characterized in breast cancer cells and normal human mammary epithelial cells (HMECs) labeled with [1,2-^{13}C]choline, using ^{1}H and ^{13}C magnetic resonance spectroscopy. Metabolic fluxes between membrane and water-soluble pool of choline-containing metabolites were assessed by exposing cells to [1,2-^{13}C]choline for long and short periods of time to distinguish between catabolic and anabolic pathways in choline metabolism. Gene expression analysis using microarrays was performed to understand the molecular mechanisms underlying these changes. Breast cancer cells exhibited increased phosphocholine (PC; $P < 0.001$), total choline-containing metabolites ($P < 0.01$), and significantly decreased glycerophosphocholine ($P < 0.05$) compared with normal HMECs. Decreased ^{13}C-enrichment was detected in choline ($P < 0.001$) and phosphocholine ($P < 0.05$, $P < 0.001$) of breast cancer cells compared with HMECs, indicating a higher metabolic flux from membrane phosphatidylcholine to choline and phosphocholine in breast cancer cells. Choline kinase and phospholipase C were significantly overexpressed, and lysophospholipase 1, phospholipase A2, and phospholipase D were significantly underexpressed, in breast cancer cells compared with HMECs. The magnetic resonance spectroscopy data indicated that elevated phosphocholine in breast cancer cells was primarily attributable to increased choline kinase activity and increased catabolism mediated by increased phospholipase C activity. These observations were consistent with the overexpression of choline kinase and phospholipase C detected in the microarray analyses.

INTRODUCTION

Over the past decade, one common feature consistently revealed by magnetic resonance (MR) spectroscopic studies is the elevation of phosphocholine (PC) and total choline-containing metabolites [tCho, glycerophosphocholine (GPC)+PC+free choline (Cho)] in cancer cells and solid tumors. Clinical magnetic resonance spectroscopy (MRS), particularly ^{1}H MRS imaging, is attracting a high level of interest as a method to detect the extent of invasion of brain tumors (1), as well as prostate (2) and breast cancer (3), and to differentiate between recurrence or necrosis after treatment (2, 4). Our purpose in this study was to delineate molecular mechanisms underlying the altered choline phospholipid metabolism typically observed in breast cancer cells; the identification of these mechanisms would further our understanding of tumor biology and uncover unique targets to exploit for therapy.

The aberrant choline phospholipid metabolism of breast cancer cells and its strong correlation with malignant progression has been observed in several studies. Human breast cancer cells in culture exhibit consistently elevated PC levels (5, 6). A step-wise increase of PC and total choline-containing metabolites was observed in immortalized, oncogene-transformed, or tumor-derived human mammary epithelial cells (HMECs; Ref. 7) used as a model of breast cancer progression. Highly malignant breast cancer cells that were transfected with the metastasis suppressor gene *nm23* exhibited a significantly lower ratio of PC to GPC compared with empty vector-transfected control cells and tumors (8). An increase in PC levels was detected in NIH 3T3 cells transfected with mutant *ras*-oncogene as compared with the parental cell line (9). Antimicrotubule drugs, such as the anticancer drug paclitaxel, vincristine, colchicine, and nocodazole, induced a significant increase of cellular GPC levels in several breast cancer cell lines (10). An increase of GPC and a decrease of PC were also detected in malignant HMECs after treatment with the nonsteroidal anti-inflammatory agent indomethacin (11). Collectively, these data indicate that diverse molecular alterations and treatments arrive at common end points in choline phospholipid metabolism of breast cancer. Aberrant choline phospholipid metabolism has also been demonstrated in inflammation-related pathologies (12, 13) and neurological disorders, such as multiple sclerosis (14), Alzheimer's disease (15), and Gaucher's disease (16). Apoptosis has been linked to altered choline phospholipid metabolite concentrations as well (17). As shown in the schematic in Fig. 1, choline phospholipid metabolism consists of a complex ensemble of biosynthetic pathways and catabolic breakdown pathways, with one or more enzymes acting per pathway. Identifying the molecular causes of the differences in choline phospholipid metabolism between normal HMECs and breast cancer cells would be advantageous for several reasons. For diagnostic MRS applications, it is necessary to understand why cancer cells exhibit this typical alteration of choline phospholipids. Such an understanding can also potentially provide novel targets for cancer treatment. When using MRS to follow tumor response to therapy, it is necessary to understand the relationship between the target of chemotherapy and the pathways leading to a certain end point in choline phospholipid metabolism detectable by MRS.

Previous studies have demonstrated the utility of [1,2-^{13}C]choline in combination with ^{13}C MR spectroscopy to study choline metabolism (18, 19). In this study, ^{1}H and ^{13}C MR spectroscopy of cells labeled with [1,2-^{13}C]choline was performed to further understand mechanisms underlying the differences in choline phospholipid metabolism of malignant breast cancer cells *versus* HMECs. The spontaneously immortalized, nonmalignant HMEC line MCF-12A was compared with the estrogen receptor-negative, highly metastatic/invasive human breast cancer line MDA-MB-231. Long-term and short-term steady-state exposure with [1,2-^{13}C]choline were performed to distinguish between anabolic and catabolic pathways of choline metabolism. This approach was used to detect differences in the relative metabolic fluxes between HMECs and human breast cancer cells. A microarray-based gene expression analysis using the human genome U133 GeneChip set from Affymetrix was performed to probe >39,000 transcripts derived from approximately 33,000 well-substantiated human genes. This microarray analysis was used to determine

Received 12/8/03; revised 3/19/04; accepted 4/14/04.

Grant support: This work was supported by NIH 2R01 CA82337, P50 CA103175.

The costs of publication of this article were defrayed in part by the payment of page charges. This article must therefore be hereby marked *advertisement* in accordance with 18 U.S.C. Section 1734 solely to indicate this fact.

Requests for reprints: Zaver M. Bhujwalla, Department of Radiology, Johns Hopkins University School of Medicine, 208C Traylor Building, 720 Rutland Avenue, Baltimore, MD 21205. Phone: (410) 955-9698; Fax: (410) 614-1948; E-mail: zaver@mri.jhu.edu.

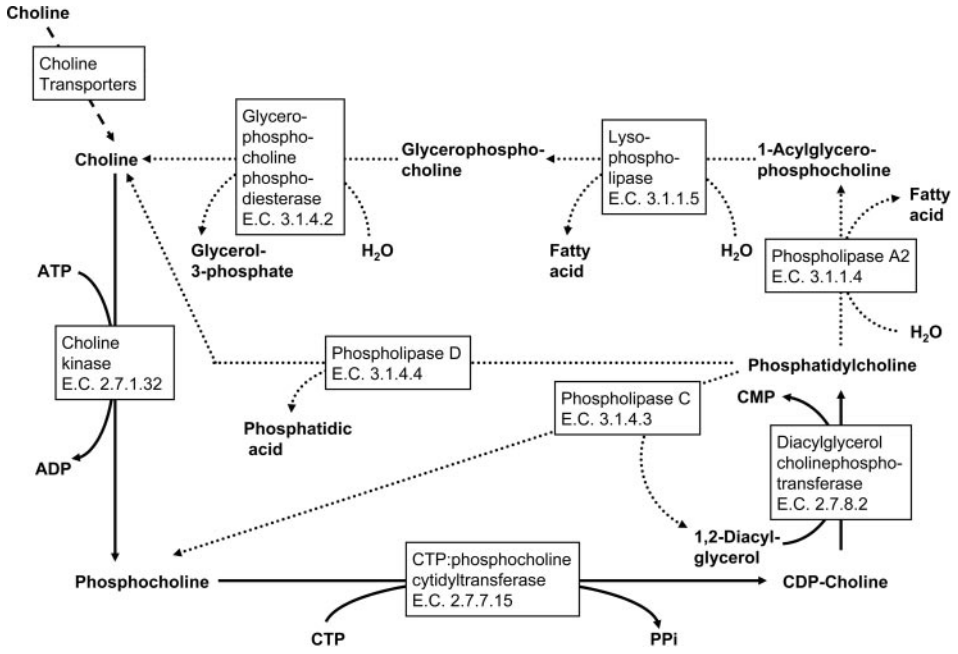

Fig. 1. Biosynthetic (*solid lines*) and catabolic (*dashed lines*) pathways of phosphatidylcholine metabolism. CDP, cytosine diphosphate; CMP, cytosine monophosphate; CTP, cytosine triphosphate; PPi, pyrophosphate.

differences in the gene expression profiles of nonmalignant HMECs MCF-12A *versus* highly metastatic MDA-MB-231 breast cancer cells.

MATERIALS AND METHODS

Cell Lines. Models representing human mammary epithelium and human breast cancer cells were used in this study. MCF-12A, a spontaneously immortalized nonmalignant cell line established from MCF-12M mortal cells (20), was used as a model of normal human mammary epithelium. MCF-12A cells were obtained from American Type Culture Collection (Rockville, MD) and cultured in DMEM-Ham's F12 medium (Invitrogen Corp., Carlsbad, CA) supplemented as described previously (20). MDA-MB-231, a highly metastatic human mammary epithelial cancer cell line, was used as a model of human breast cancer cells. MDA-MB-231 cells were provided by Dr. R. J. Gillies (Arizona Health Sciences Center, Tuscon, AZ) and maintained in RPMI 1640 (Invitrogen Corp.) supplemented with 10% fetal bovine serum, 100 units/ml penicillin, and 100 μg/ml streptomycin (Invitrogen Corp.). This human breast adenocarcinoma cell line was originally isolated from a pleural effusion of a patient with breast cancer. All cells were maintained in a humidified atmosphere of 5% CO_2 in air, at 37°C. Both cell lines were cultured in media containing approximately 20 μM choline.

Incubation and Dual Phase Extraction. MCF-12A and MDA-MB-231 cells were cultured to 60% confluence. Long-term and short-term labeling experiments with [1,2-^{13}C]choline were performed for both cell lines to distinguish between the anabolic and catabolic pathways in choline phospholipid metabolism. In long-term experiments, cells were exposed to fresh cell culture medium containing 100 μM [1,2-^{13}C]choline (99% ^{13}C-enriched; Cambridge Isotope Laboratories, Inc., Andover, MA) for a total time period of 27 h, including a medium exchange after 24 h to provide fresh medium containing 100 μM [1,2-^{13}C]choline for the last 3 h of exposure. This long-term [1,2-^{13}C]choline exposure resulted in a partially enriched ^{13}C membrane phosphatidylcholine (PtdCho) pool. In short-term experiments, cells were exposed to fresh cell culture medium containing 100 μM unlabeled choline for 24 h, followed by a 3-h incubation with 100 μM [1,2-^{13}C]choline in fresh cell culture medium. After this short-term [1,2-^{13}C]choline exposure, cells had an unlabeled membrane PtdCho pool. These higher extracellular choline levels (100 μM) during short- and long-term labeling did not significantly alter the ^{1}H MRS-detectable choline metabolite concentrations. Choline metabolite concentrations detected in the present study were comparable with concentrations detected in earlier studies (7) using 20 μM concentration of Cho in the medium.

After the experimental incubations, approximately 10^8 cells were harvested and both lipid and water-soluble cell extract fractions were obtained using a dual-phase extraction method as described previously (21). Briefly, 10^7-10^8 cells/ extract were harvested by trypsinization, washed twice with 10 ml of saline at room temperature, and pooled into a glass centrifuge tube. Cells were counted for quantitation directly after trypsinization. Four ml of ice-cold methanol were added to the cells, vigorously vortexed, and kept on ice for 10 min. Four ml of chloroform were added and vigorously vortexed. Finally, 4 ml of water were added, the sample was vortexed and left overnight at 4°C for phase separation. The samples were centrifuged for 30 min at 35,000 $\times$ *g* at 4°C, and the phases were carefully separated. The water-methanol phase containing the water-soluble cellular metabolites was treated with 10 mg of chelex for 10 min on ice to remove divalent cations. The chelex beads were then removed. Methanol was removed by rotary evaporation. The remaining water phases were lyophilized and stored at -20°C. The chloroform phase containing the cellular lipids was dried in a stream of N_2 and stored under N_2 at -20°C.

NMR Data Acquisition and Processing. The water-soluble samples were dissolved in 0.5 ml of D_2O (Sigma-Aldrich, St. Louis, MO) containing 0.24×10^{-6} mol 3-(trimethylsilyl)propionic-2,2,3,3,-d_4 acid (Sigma-Aldrich) as an internal concentration standard (sample pH of 7.4). The lipid samples were dissolved in 0.6 ml of $CDCl_3/CD_3OD$ (2:1, v/v) containing 2.17×10^{-6} mol tetramethylsilane as an internal concentration standard ($CDCl_3$ and CD_3OD were premixed with tetramethylsilane by the manufacturer, Cambridge Isotope Laboratories, Inc.). High-resolution ^{1}H-decoupled ^{13}C and fully relaxed ^{1}H MR spectra of the extracts were acquired on a Bruker MSL-500 spectrometer operating at 11.7 Tesla (Bruker BioSpin Corp., Billerica, MA). Fully relaxed ^{1}H MR spectra (without saturation effects) of water-soluble metabolites and lipids were obtained at 500 MHz using a 5-mm HX inverse probe and the following acquisition parameters: 30° flip angle, 6000 Hz sweep width, 12.7 s repetition time, time-domain data points of 32K, and 128 transients. Composite pulse (WALTZ-16) ^{1}H-decoupled ^{13}C MR spectra of the water-soluble metabolites and lipids were recorded at 125.7 MHz, using a 10-mm broadband probe, 30° flip angle, 29411 Hz sweep width, 3 s repetition time, time-domain data points of 16K (zero-filled to 32K before Fourier transform), and 20,000 transients for water-soluble metabolites or 6000 transients for lipids. The ^{13}C MR spectra of water-soluble metabolites and lipid samples were corrected for saturation effects and Nuclear Overhauser effect. Partially saturated spectra of control cells acquired with Nuclear Overhauser effect were compared to spectra of identical samples acquired under fully relaxed conditions (6 s repetition time) without Nuclear Overhauser effect using inverse-gated decoupling.

All spectra were analyzed using an in-house software program, Soft Fourier Transform (P. Barker, The Johns Hopkins University School of Medicine). The

signals of 3-(trimethylsilyl)propionic-2,2,3,3,-d_4 acid (water-soluble metabolites) or tetramethylsilane (lipids) served as references for chemical shift and concentration in the ^{1}H MR spectra. The signal integrals of the N-$(CH_3)_3$ signals of Cho at 3.209 parts/million (ppm), PC at 3.227 ppm, and GPC at 3.236 ppm in the ^{1}H MR spectra of water-soluble metabolites as well as the N-$(CH_3)_3$ signal of PtdCho at 3.22 ppm in the ^{1}H MR spectra of lipids were determined and normalized to cell size and number as described previously (7) using the following equation:

$$[\text{metabolite}] = \{I(\text{metabolite}) \times \text{standard}\}/\{I(\text{standard}) \times \text{cell number} \times \text{cell volume}\}$$

In this equation, [metabolite] represents the intracellular concentration of the metabolite of interest expressed in mM, I(metabolite) represents the signal integral of the metabolite of interest divided by the number of protons, and (standard) represents the amount of 3-(trimethylsilyl)propionic-2,2,3,3,-d_4 acid (water-soluble metabolites) or tetramethylsilane (lipids) used in mol divided by the number of protons. The number of cells in each sample (cell number) was counted before extraction, and the cell volume values used were determined previously for MCF-12A and MDA-MB-231 cells (7). Long-term and short-term [1,2-^{13}C]choline exposure experiments did not significantly alter total metabolite concentrations as quantitated from ^{1}H MR spectra. Therefore, data from these experiments were pooled.

^{13}C MR spectra of water-soluble metabolites were referenced to the lactate C3 signal at 21.3 ppm. The lipid ^{13}C MR spectra were calibrated using the solvent signal of deuterated methanol at 49.5 ppm. The corrected ^{13}C signal integral of the N-$(CH_3)_3$ group signal at 55.0–55.2 ppm was used as a reference to calculate the ^{13}C-enrichment of Cho, PC, GPC, and PtdCho. This was possible because the corrected ^{13}C signal integral of the N-$(CH_3)_3$ group contained only the natural abundance ^{13}C-signal contribution of Cho+PC+GPC (water-soluble metabolites) or PtdCho (lipids). A value of 1.07% was used for the natural abundance of the ^{13}C isotope of carbon. The N-$(CH_3)_3$ group signal was chosen for this purpose because it was detected in the ^{1}H as well as in the ^{13}C MR spectra. Calculation of the fractional ^{13}C-enrichments was performed with the signals of GPC, PC, and Cho within the O-CH_2 region because, unlike the N-CH_2 region, there was no signal overlap in this region. Both signals of PtdCho were used for analysis in the lipid ^{13}C MR spectra. The fractional ^{13}C-enrichments were calculated from the corrected ^{13}C signal integrals of Cho, PC, GPC, and N-$(CH_3)_3$ in the spectra of water-soluble metabolites, and PtdCho and N-$(CH_3)_3$ in the lipid spectra according to the following equation:

$$\text{Fractional } ^{13}\text{C-enrichment(metabolite)} = \{\text{I-}^{13}\text{C(metabolite)} \times \text{I-}^{1}\text{H(N-(CH}_3)_3) \times 0.0107\}/\{\text{I-}^{13}\text{C(N-(CH}_3)_3) \times \text{I-}^{1}\text{H(metabolite)}\}$$

In this equation, ^{13}C-enrichment(metabolite) represents the fractional ^{13}C-enrichment within the total pool of the metabolite of interest, I-^{13}C(metabolite) represents the signal integral of the metabolite of interest in the ^{13}C MR spectrum divided by the number of carbons, I-^{1}H(N-$(CH_3)_3$) represents the signal integral of the N-$(CH_3)_3$-signal of (Cho+PC+GPC) or PtdCho in the ^{1}H MR spectrum divided by the number of protons, I-^{13}C(N-$(CH_3)_3$) represents the signal integral of the natural abundance N-$(CH_3)_3$ signal of (Cho+PC+GPC) or PtdCho at 55.0–55.2 ppm divided by the number of carbons, and I-^{1}H(metabolite) represents the signal integral of the metabolite of interest in the ^{1}H MR spectrum divided by the number of protons.

Statistical Analysis of MR Experiments. An unpaired 2-tailed *t* test ($\alpha = 0.05$) was used to detect significant differences between HMECs and breast cancer cells. Because comparable metabolite concentrations, within the SDs, were obtained in the ^{1}H MR spectra of the long-term ($n = 3$) and the short-term ($n = 3$) [1,2-^{13}C]choline exposure, ^{1}H MR data from these experiments were pooled to give $n = 6$. *P*s of <0.05 were considered to be significant.

Total RNA Isolation and GeneChip Microarray Assay. Total cellular RNA was isolated from approximately 10^7 MDA-MB-231 or MCF-12A cells using the RNeasy Mini Kit (Qiagen Inc., Valencia, CA). Experiments were performed in duplicates. Cells were washed twice with PBS and immediately lysed using 600 μl of RTL lysis buffer containing 6-μl β-mercaptoethanol. Samples were transferred to QIAshredder homogenizer spin columns (Quiagen Inc.) and homogenized. Total cellular RNA was isolated according to the manufacturer's protocol (RNeasy Mini Kit). The concentration and purity of the RNA samples was assessed by measurement of the UV absorption (Beckman Coulter Inc., Fullerton, CA) at 260 nm and the absorption ratio of 260 to 280 nm, respectively. The integrity and size distribution of the total RNA preparations was checked by formaldehyde-agarose gel electrophoresis that was performed using the buffer preparations suggested in the RNeasy Mini handbook. RNA samples were stored at −70°C.

The microarray hybridization was performed at the JHMI Microarray Core Facility (Dr. Francisco Martinez Murillo, Johns Hopkins University School of Medicine) using the Human Genome U133 Set consisting of two GeneChip arrays (Affymetrix Inc., Santa Clara, CA) and the Affymetrix GeneChip platform. The Human Genome U133 GeneChip Set (U133 A and B) contains approximately 45,000 probe sets that represent 39,000 transcripts. Briefly, 10 μg of the purified total RNA were converted to cDNA. This first strand cDNA was synthesized using oligonucleotide probes with the 24 oligodeoxythymidylic acid plus T7 promoter as primer and the SuperScript Choice System (Life Technologies, Inc. Invitrogen Corp.). After synthesis of double-stranded cDNA, biotinylated antisense cRNA was generated by in *vitro* transcription using the BioArray RNA High Yield Transcript Labeling kit (ENZO Life Sciences, Enzo Biochem Inc., New York, NY). Fifteen μg of the biotinylated cRNA was fragmented at 94°C for 35 min and hybridized to the GeneChip array for 16 h at 45°C with constant rotation (60 rpm). An Affymetrix Fluidics Station 400 was used to wash the GeneChip and to remove the nonhybridized target, followed by incubation with a streptavidin-phycoerythrin conjugate to stain the biotinylated cRNA. Fluorescence from the GeneChip was detected using the Agilent GeneArray Scanner and the Micro Array Suite 5.0 software (Affymetrix).

Analysis of Microarray Data. For comparison between different samples, the intensity values for a given probe on the Affymetrix GeneChip array (cell intensity) were normalized by the method of "invariant set normalization" (22). This method is based on the similar overall brightness of the scanned U133 A and B GeneChip images across samples because only a small fraction of genes is differentially expressed in different cell lines of the same tissue type. A high correlation ($\geq$0.92) was detected between the chips, which was consistent with this assumption. For the same reason, the scanned images of the chips should have a similar overall brightness. To adjust the brightness between the sample chips to a comparable level, a subset of perfect match probes with small within-subset rank difference between the chips was chosen by an iterative procedure to serve as the basis for fitting a normalization curve. The U133 A and B chips most representative of the median overall brightness (median cell intensity) among the two groups of U133 A and B chips were used as the baseline chips for normalization. An example of the scatter plot of this normalization is shown in Fig. 2, where the normalization curve of the running median shows some deviation from the diagonal reference line of y = x, which suggests that there is a need for normalization (*i.e.*, one chip is brighter than the other). The normalized cell intensity data were then used to estimate the perfect-match/mismatch-model-based expression index (with SEs) for the probe sets of various samples. Fold changes and their 90% confidence intervals between the samples were computed based on the estimates of the expression index and the corresponding SEs (23). The lower boundary of a 90% confidence interval, a conservative estimate of the fold change, or the fold change itself was then used to identify differentially expressed genes (*i.e.*, up-regulated or down-regulated genes; Ref. 23). The computing work described above was performed with the software package of dChip (22).

RESULTS

Several differences in choline metabolite levels and metabolic fluxes between HMECs and human breast cancer cells were apparent in the ^{13}C and ^{1}H MR spectra. Typical ^{13}C spectra of water-soluble metabolites obtained from MCF-12A HMECs (*bottom panel*) and MDA-MB-231 human breast cancer cells (*top panel*) after long-term or short-term exposure to [1,2-^{13}C]choline are shown in Fig. 3, *A* and *B*, respectively. The corresponding ^{1}H MR spectra are shown in Fig. 3*C*. [1,2-^{13}C]choline was transported into the cells and metabolized to the intracellular water-soluble metabolites PC and GPC. The two ^{13}C methylene signals in the N-CH_2 and the O-CH_2 group of Cho, PC, and

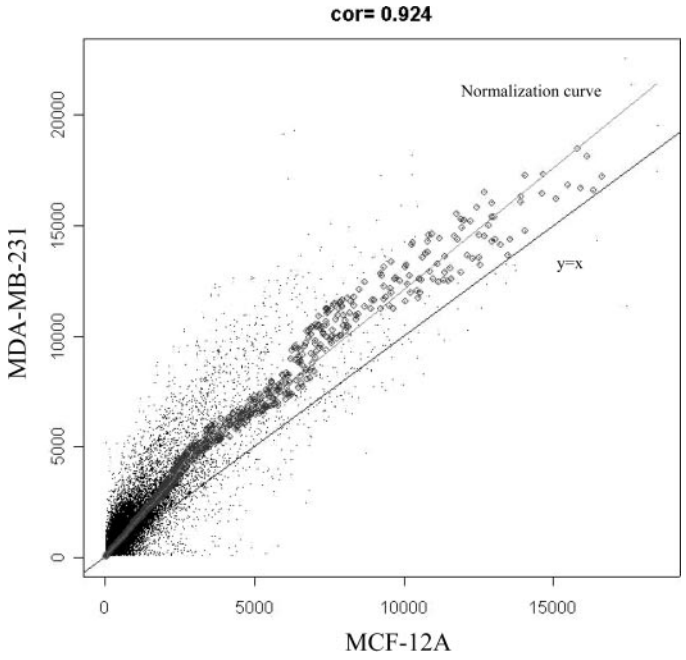

Fig. 2. Scatter plot of the perfect match (PM) and mismatch (MM) data between two GeneChip samples obtained from MCF-12A and MDA-MB-231 cells. The normalization curve of the running median is based on the "invariant set" of PM points, which has a small within-subset rank difference and is represented by the *open circles*. The *diagonal line* of y = x is also shown as a reference. Cor = 0.924 is the sample correlation coefficient between the data points of the two samples.

GPC were observed in the long-term ^{13}C MR spectra of both cell lines (Fig. 3*A*). These two ^{13}C-labeled methylene carbons in metabolites formed using [1,2-^{13}C]choline exhibited chemical shifts at 56.8 and 68.6 ppm in [1,2-^{13}C]Cho, 59.2 and 67.7 ppm in [1,2-^{13}C]PC, and 60.6 and 67.2 ppm in [1,2-^{13}C]GPC, as well as distinct coupling patterns. Because the functional group in the three choline-metabolites PC, GPC, and PtdCho is attached to the ^{13}C-labeled O-CH_2 group, this ^{13}C-labeled carbon has the largest chemical shift differences between the three different choline metabolites. The characteristic $^1J_{CC}$ coupling constant of about 37.5–39.5 Hz allows resolution of ^{13}C-labeled and unlabeled molecules. Choline metabolites carrying a phosphate group (PC, GPC, PtdCho) exhibit another doublet $^2J_{PC}$ coupling pattern, which is of the order of 4–5 Hz. The ^{13}C-labeled N-CH_2 carbon signal is additionally split into a multiplet through coupling with ^{14}N. This causes broader signals, resulting in an overlap between PC and GPC. Therefore, signals from the O-CH_2 region were used for quantifying ^{13}C-enrichment. Representative ^{13}C MR spectra of the corresponding lipid fractions, obtained from MCF-12A cells (*bottom panel*), and MDA-MB-231 cells (*top panel*), after long-term or short-term exposure to [1,2-^{13}C]choline are shown in Fig. 4, *A* and *B*, respectively. Two ^{13}C methylene signals in the N-CH_2 group (67.4 ppm) and the O-CH_2 group (59.8 ppm) of membrane PtdCho were detected in the long-term experiments as shown in Fig. 4*A*. The signals were split to a doublet or a doublet of doublets by $^1J_{CC}$ and/or $^2J_{PC}$ couplings.

^{1}H MR spectra in Fig. 3*C* demonstrate that HMECs contained low PC in contrast to the high PC levels observed in the breast cancer cell line. Concentrations of metabolites derived from the ^{1}H MR spectra of water-soluble and lipid fractions are summarized in Fig. 5*A* ($n = 6$). Breast cancer cells exhibited significantly increased PtdCho ($P < 0.05$, $n = 6$), PC ($P < 0.001$, $n = 6$), and tCho ($P < 0.01$, $n = 6$) levels and significantly decreased GPC levels ($P < 0.05$, $n = 6$) compared with HMECs. Consequently, the PC/GPC ratio was significantly ($P < 0.001$, $n = 6$) higher in breast cancer cells (PC/GPC ratio of 4.83 ± 0.75, $n = 6$) compared to HMECs (PC/GPC ratio of 0.24 ± 0.04, $n = 6$). No significant differences were detected in Cho levels ($n = 6$). Extracellular choline levels of 100 μM used during the experimental incubations in the present study did not significantly affect the ^{1}H MRS-detectable choline metabolite concentrations. The choline metabolite concentrations detected in the present study are comparable to concentrations detected in earlier studies (7), where experiments were performed in cell culture medium containing 20 μM extracellular choline.

Relative metabolic fluxes between the membrane pool and the water-soluble pool of choline-containing metabolites were assessed from the spectra of cells exposed to [1,2-^{13}C]choline for a long or short duration. In the long-term experiments, a ^{13}C-labeled PtdCho pool built up during the 27 h labeling period with [1,2-^{13}C]choline, contributed to the incorporation of ^{13}C-label into the water-soluble choline-containing metabolites through catabolic pathways. This was evident from the appearance of the two ^{13}C methylene signals in membrane PtdCho detected in the long-term experiments of both cell lines as shown in Fig. 4*A*. No significant difference in the fractional ^{13}C-enrichment of PtdCho was detected between HMECs and breast cancer cells after 27 h (24 h + 3 h) of exposure to [1,2-^{13}C]choline; the ^{13}C-enrichment of PtdCho was about 0.2 in both (Fig. 5*B*). The HMEC and breast cancer cell lines used in this study have comparable cell-doubling times (MCF-12A, 21.6 ± 0.6 h; MDA-MB-231, 28.6 ± 1.0 h) as reported previously (7). In contrast, short-term experiments, where unlabeled choline was administered during the 24 h prelabeling period, resulted in nondetectable [1,2-^{13}C]PtdCho levels in both cell lines as demonstrated in the short-term ^{13}C MR

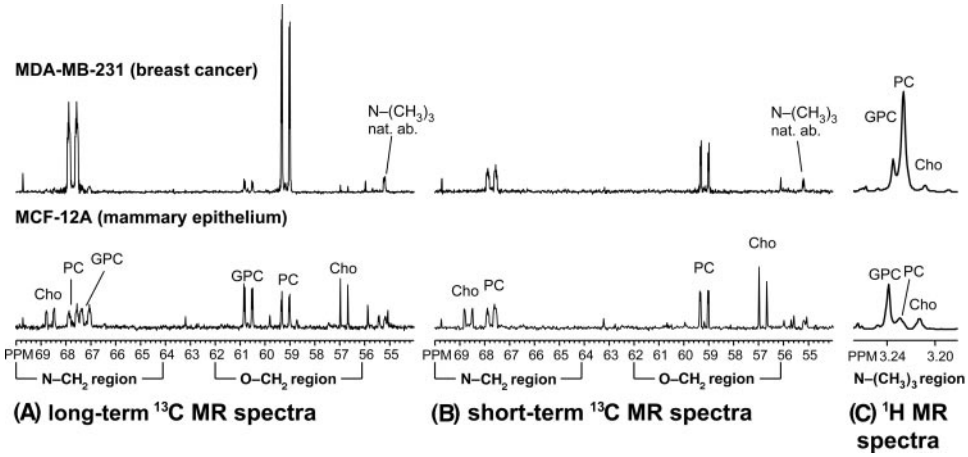

Fig. 3. Representative (*A*) long-term ^{13}C, (*B*) short-term ^{13}C, and (*C*) ^{1}H MR spectra of the water-soluble fractions of human mammary epithelial cells (MCF-12A, *bottom panel*), and human breast cancer cells (MDA-MB-231, *top panel*). MDA-MB-231 and MCF-12A cells were labeled with 100 μM [1,2-^{13}C]choline for 24 h + 3 h in the long-term experiments and for 3 h in the short-term experiments. *MR*, magnetic resonance

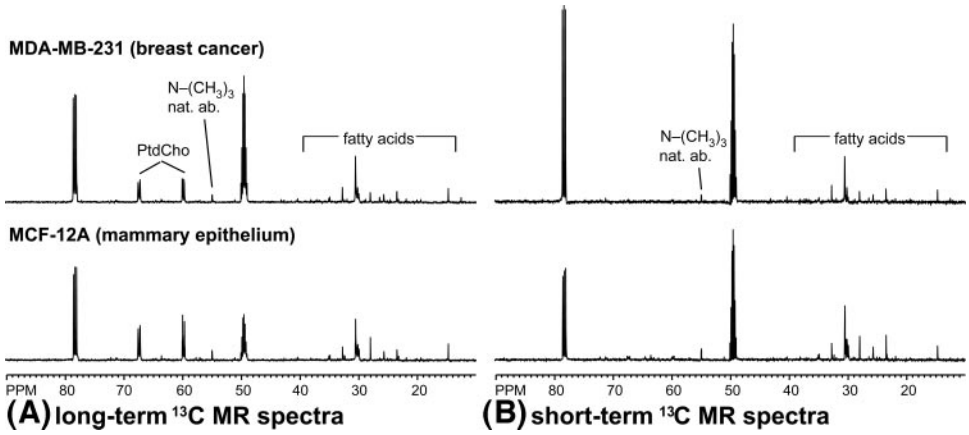

Fig. 4. Representative (*A*) long-term and (*B*) short-term ^{13}C MR spectra of the lipid fractions of human mammary epithelial cells (MCF-12A, *bottom panel*), and human breast cancer cells (MDA-MB-231, *top panel*). MDA-MB-231 and MCF-12A cells were labeled with 100 μM [1,2-^{13}C]choline for 24 h + 3 h in the long-term experiments and for 3 h in the short-term experiments. *MR*, magnetic resonance.

spectra in Fig. 4*B*. Consequently, ^{13}C-enrichment in the water-soluble metabolites of long-term experiments was generated by a combination of biosynthetic plus catabolic pathways, whereas ^{13}C-enrichment in the water-soluble metabolites of short-term experiments was generated by biosynthetic pathways alone. Thus, a comparison between long-term and short-term experiments enabled us to estimate relative contributions from biosynthesis and breakdown of PtdCho (Fig. 1) to the Cho, PC, and GPC pools observed in HMECs and breast cancer cells.

As shown in Fig. 5*B*, ^{13}C-enrichment of Cho (long-term and short-term, $P < 0.001$, $n = 3$) and PC (long-term, $P < 0.05$, $n = 3$; short-term, $P < 0.001$, $n = 3$) was significantly lower in breast cancer cells compared with HMECs ($n = 3$). This was most likely because the partially labeled (long-term experiments) or unlabeled (short-term experiments) PtdCho pool was breaking down at a higher rate into Cho and PC in the breast cancer cells. In breast cancer cells, the ^{13}C-enrichment in Cho was significantly higher ($P < 0.01$, $n = 3$; Fig. 5*B*) in long-term compared with short-term labeling experiments, but it was the same for long and short-term experiments in HMECs (Fig. 5*B*; $n = 3$). This demonstrates that the difference in ^{13}C-enrichment of membrane PtdCho in both HMECs and breast cancer cells between long-term (approximately 0.2) *versus* short-term (approximately 0.0) experiments (Figs. 4 and 5*B*) was reflected by a corresponding difference in the ^{13}C-enrichment in Cho in breast cancer cells (Fig. 5*B*; long-term Cho, 0.2 $\pm$ 0.05, $n = 3$; short-term Cho, 0.0 $\pm$ 0.04, $n = 3$) but not in HMECs (Fig. 5*B*; long-term Cho, 0.68 $\pm$ 0.11, $n = 3$; short-term Cho, 0.72 $\pm$ 0.12, $n = 3$). Thus, the contribution of Cho from the breakdown of PtdCho was significantly lower in HMECs. In contrast, this contribution played a major role in breast cancer cells, as indicated by nondetectable levels of ^{13}C-labeled Cho in the short-term experiments.

The ^{13}C-enrichment of PC was significantly ($P = 0.01$, $n = 3$) higher in the long-term as compared with short-term [1,2-^{13}C]choline exposure in the breast cancer cells (Fig. 5*B*; $n = 3$) but not in the HMECs (Fig. 5*B*; $n = 3$) where it was equal. Thus, breakdown of PtdCho, in addition to the biosynthetic pathway, played a significant role in the build-up of the PC pool in breast cancer cells; in HMECs, PC was primarily generated from the action of choline kinase in the biosynthetic pathway. ^{13}C-enrichment in GPC was only detected in the long-term [1,2-^{13}C]choline exposure experiments of breast cancer cells and HMECs (Figs. 3*A* and 5*B*; $n = 3$), but not in short-term experiments (Figs. 3*B* and 5*B*; $n = 3$). Therefore, GPC was exclusively derived from catabolic breakdown pathways in breast cancer cells and HMECs. No significant difference in ^{13}C-enrichment of GPC was detected between breast cancer cells and HMECs (Fig. 5*B*; $n = 3$).

Several differences in gene expression were detected between MDA-MB-231 breast cancer cells and MCF-12A HMECs by mRNA

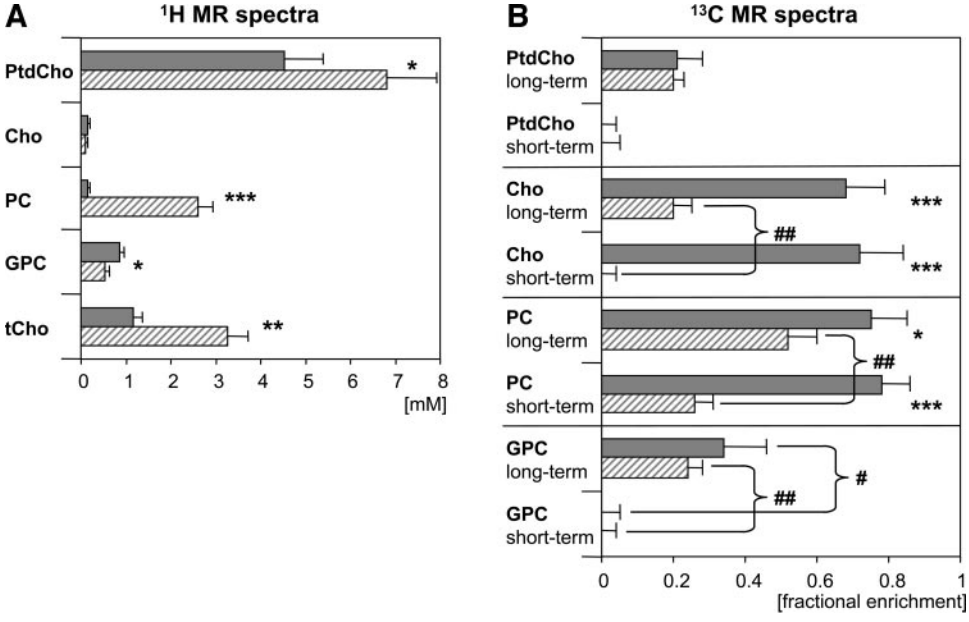

Fig. 5. *A*, PtdCho, Cho, PC, GPC, and tCho levels in human mammary epithelial cells (MCF-12A, *solid bars*) and breast cancer cells (MDA-MB-231, *striped bars*) quantified from ^{1}H MR spectra. Because equal metabolite concentrations within the SDs were detected in ^{1}H MR spectra after long-term ($n = 3$) or short-term ($n = 3$) [1,2-^{13}C]choline exposure, ^{1}H MR data from these experiments were pooled to give $n = 6$. PtdCho, phosphatidylcholine; Cho, free choline; *PC*, phosphocholine; GPC, glycerophosphocholine; tCho, total choline-containing metabolites (GPC+PC+Cho). *B*, quantitation of the fractional ^{13}C-enrichment in PtdCho, Cho, PC, and GPC from long-term experiments ($n = 3$) and short-term ($n = 3$) experiments in HMECs (MCF-12A, *solid bars*) and breast cancer cells (MDA-MB-231, *striped bars*). Values represent mean $\pm$ SD, * indicates $P < 0.05$, ** indicates $P < 0.01$, *** indicates $P < 0.001$ for MCF-12A *versus* MDA-MB-231, # indicates $P < 0.05$, ## indicates $P < 0.01$ for long-term *versus* short-term. *MR*, magnetic resonance.

analysis using the Affymetrix human genome U133 A and B GeneChips combined with statistically modeled probe-level data analysis (22, 23). A total of 1085 transcripts and 60 expressed sequence tags of >39,000 transcripts were differentially expressed in breast cancer cells *versus* HMECs, using the lower boundary of a 90% confidence interval of the 2-fold overexpression or underexpression. Differentially expressed genes involved in choline phospholipid metabolism are listed in Table 1. All of the known genes of enzymes involved in choline metabolism were represented on the Affymetrix human genome U133 A/B GeneChip set. The genes for GPC-phosphodiesterase (E.C. 3.1.4.2) have not been discovered yet. Therefore, gene expression of GPC-phosphodiesterase was not tested with the human genome U133 A/B GeneChip set. Choline kinase (NM_001277), and two different phospholipase C genes, pancreas-enriched phospholipase C (NM_016341) and phospholipase C β 3 neighbor pseudogene (Hs.100623) were significantly overexpressed in breast cancer cells. Lysophospholipase 1 (NM_006330), phospholipase A2 group IVA (cytosolic, calcium-dependent, NM_024420), and phospholipase D (NM_002662) were significantly underexpressed in breast cancer cells compared with HMECs. Overexpression of choline kinase and underexpression of lysophospholipase 1 were consistently detected with two different probe sets each. Overexpression of choline kinase in MDA-MB-231 breast cancer cells *versus* MCF-12A HMECs was additionally verified by reverse transcriptase PCR (data not shown). All known choline transporter genes, such as the high affinity choline tranporter CHT1, the antigen CDw92 CLT-1, and the organic cation transporters OCT-1/-2 were equally expressed in breast cancer cells compared to HMECs.

DISCUSSION

Several molecular mechanisms responsible for the altered choline metabolism of breast cancer cells were identified in this combined MRS and microarray analyses study. The main observations of the microarray analyses were overexpression of choline kinase and phospholipase C and reduced expression of lysophospholipase 1, phospholipase A2, and phospholipase D1 in MDA-MB-231 breast cancer cells compared with MCF-12A HMECs. Most of the differences in gene expression were consistent with the differences detected by ^{1}H and ^{13}C MR spectroscopy. Increased intracellular PC and PtdCho levels and a decreased GPC concentration in breast cancer cells compared with HMECs was detected by ^{1}H MRS. Differences in relative metabolic choline fluxes between HMECs *versus* breast cancer cells were determined by comparing long-term and short-term incubations with [1,2-^{13}C]choline using ^{13}C MRS. This ^{13}C MRS approach revealed that breakdown of membrane phosphatidylcholine contributed substantially to the increased PC levels in breast cancer cells, indicating increased phospholipase C and/or D activity in these cancer cells. Breakdown of membrane phosphatidylcholine also contributed to Cho levels in breast cancer cells to a greater extent than in HMECs. Thus, the application of two independent methods, ^{1}H/^{13}C MRS and microarray analysis, revealed that a combination of increased choline kinase and increased phospholipase D and/or C expression/activity caused the elevated PC levels in breast cancer cells.

These results are also consistent with previous studies which demonstrated that breast cancer cells exhibited a high rate of choline phosphorylation by choline kinase (24, 25). HMECs, in comparison, revealed equally low cellular PC and Cho levels indicative of a low choline kinase expression and/or activity. Thus, the increased tCho levels in breast tumors detected in the clinic are primarily because of high PC levels. This is further supported by studies demonstrating that the enzymatic activity of choline kinase is associated with histological tumor grade and ER-negative tumors (25).

The ^{13}C MRS data revealed significant differences in the fractional enrichment of Cho and PC between MDA-MB-231 breast cancer cells and MCF-12A HMECs. There was no detectable ^{13}C labeling of PtdCho in MCF-12A HMECs in the short-term experiments. However, the fractional enrichments of the Cho and PC pool in the short-term experiments were similar to those in the long-term experiments in MCF-12A HMECs. In MDA-MB-231 breast cancer cells, on the other hand, the fractional ^{13}C-enrichment of the Cho and PC pool was significantly lower in the short-term experiments than in the long-term experiments. This reflects a lower or negligible contribution of phospholipase C-mediated PC, and phospholipase D-mediated Cho from PtdCho breakdown in HMECs, compared with breast cancer cells. Whereas phospholipase C expression was lower in HMECs compared with breast cancer cells, phospholipase D expression was not. The overexpression of phospholipase D in breast cancer cells reported previously (26) was not confirmed in the present study. Because microarray analyses determine gene expression and not enzyme activity, it is possible that an increase in phospholipase D enzyme activity may have led to a higher rate of formation of Cho from PtdCho (27).

Both ^{1}H and ^{13}C MR spectra demonstrated that breast cancer cells contained significantly decreased GPC levels from catabolic origin as compared with HMECs. These findings are in excellent agreement with our previous studies (7) linking malignant transformation of HMECs to an increase of PC and a decrease of GPC, resulting in an increase of the PC/GPC ratio and tCho levels (7). These decreased GPC levels were consistent with the underexpression of cytosolic, calcium-dependent phospholipase A2 group IVA and lysophospholipase 1 in breast cancer cells detected by gene expression analysis on microarrays. Although we consistently detected an underexpression of cytosolic, calcium-dependent phospholipase A2 group IVA in breast cancer cells, previous studies have linked an increase in membrane-associated phospholipase A2 group II (28) or cytosolic phospholipase A2 (29) activity to oncogenic transformation and malignant potential of breast cancer cells.

The clinical importance of ^{1}H MRS of choline compounds in breast cancer diagnosis has been demonstrated in studies *in vivo* (3, 30) and in excised breast tissue (31). It is therefore critically important to delineate the precise molecular causes and pathways leading to the observed differences in choline phospholipid metabolism between

Table 1 *Gene expression differences in MDA-MB-231 breast cancer cells versus MCF-12A human mammary epithelial cells*

Significantly over- or under-expressed genes (>2-fold difference) involved in choline phospholipid metabolism are listed. Only well-characterized human genes are displayed. Expression index values are mean ± SE.

Gene	MCF-12A	MDA-MB-231	Fold change (90% CI)[a]
Choline kinase (two independent probe sets)	39 ± 13	166 ± 29	4.27 (2.44 to 9.91)
Lysophospholipase 1 (two independent probe sets)	684 ± 29	174 ± 11	−3.94 (−3.47 to −4.50)
Phospholipase A2, group IVA (cytosolic, calcium-dependent)	98 ± 15	20 ± 3	−4.98 (−3.41 to −7.45)
Pancreas-enriched phospholipase C	19 ± 9	43 ± 8	2.28 (1.14 to 9.98)
Phospholipase C, β 3, neighbor pseudogene	209 ± 45	577 ± 87	2.76 (1.82 to 4.51)
Phospholipase D1 (phosphatidylcholine-specific)	35 ± 4	12 ± 4	−2.85 (−1.78 to −5.89)

[a] CI, confidence interval.

breast cancers and normal breast epithelium. Aberrant breast cancer cell choline phospholipid metabolism has been associated previously with enhanced choline transport (24), increased choline kinase activity (24, 25), as well as increased phospholipase D (26) and phospholipase A2 (29) activity. While confirming the increase in choline kinase expression, we have shown, for the first time, that phospholipase C as well as lysophospholipase play a critical role in the characteristic aberrant choline phospholipid metabolism detected in breast cancer cells. These three enzymes provide potential targets for breast cancer therapy, because elevated PC and tCho levels are strongly correlated with the malignancy of a given breast tumor (3, 7). Chemical inhibitors of choline kinase are currently being developed and tested as a novel means of chemotherapy for treating cancers (25, 32). Similarly, phospholipase C and lysophospholipase may be useful targets for antitumor therapy, which remains to be tested in the future using specific inhibitors for phospholipase C and lysophospholipase. MRS and MRSI will be extremely useful for following breast tumor response to chemotherapy with drugs targeted at enzymes in choline phospholipid metabolism.

In conclusion, this study demonstrated that a combination of choline kinase and phospholipase C overexpression is responsible for the elevated PC levels in breast cancer cells. The characteristic differences in choline membrane metabolism observed here between breast cancer cells and HMECs support further investigation of the role of choline phospholipid metabolism in primary and metastatic disease. The application of ^{13}C MR spectroscopy combined with microarray-based gene expression analysis was shown to be valuable in characterizing distinct metabolic fluxes and finding potential targets for treatment of breast cancer.

ACKNOWLEDGMENTS

We thank Drs. Francisco Martinez Murillo, Venu Raman, and Ioannis Stasinopoulos for expert technical assistance in performing the microarray experiments. We also thank Gary Cromwell for maintaining the cell lines.

REFERENCES

1. Li X, Lu Y, Pirzkall A, McKnight T, Nelson SJ. Analysis of the spatial characteristics of metabolic abnormalities in newly diagnosed glioma patients. J Magn Reson Imaging 2002;16:229–37.
2. Kurhanewicz J, Vigneron DB, Nelson SJ. Three-dimensional magnetic resonance spectroscopic imaging of brain and prostate cancer. Neoplasia 2000;2:166–89.
3. Katz-Brull R, Lavin PT, Lenkinski RE. Clinical utility of proton magnetic resonance spectroscopy in characterizing breast lesions. J Natl Cancer Inst (Bethesda) 2002;94: 1197–1203.
4. Leach MO, Verrill M, Glaholm J, et al. Measurements of human breast cancer using magnetic resonance spectroscopy: a review of clinical measurements and a report of localized 31P measurements of response to treatment. NMR Biomed 1998;11:314–40.
5. Ruiz-Cabello J, Cohen JS. Phospholipid metabolites as indicators of cancer cell function. NMR Biomed 1992;5:226–33.
6. Ting YL, Sherr D, Degani H. Variations in energy and phospholipid metabolism in normal and cancer human mammary epithelial cells. Anticancer Res 1996;16:1381–8.
7. Aboagye EO, Bhujwalla ZM. Malignant transformation alters membrane choline phospholipid metabolism of human mammary epithelial cells. Cancer Res 1999;59: 80–4.
8. Bhujwalla ZM, Aboagye EO, Gillies RJ, Chacko VP, Mendola CE, Backer JM. Nm23-transfected MDA-MB-435 human breast carcinoma cells form tumors with altered phospholipid metabolism and pH: a 31P nuclear magnetic resonance study in vivo and in vitro. Magn Reson Med 1999;41:897–903.
9. Ronen SM, Jackson LE, Beloueche M, Leach MO. Magnetic resonance detects changes in phosphocholine associated with Ras activation and inhibition in NIH 3T3 cells. Br J Cancer 2001;84:691–6.
10. Sterin M, Cohen JS, Mardor Y, Berman E, Ringel I. Levels of phospholipid metabolites in breast cancer cells treated with antimitotic drugs: a (31)p-magnetic resonance spectroscopy study. Cancer Res 2001;61:7536–43.
11. Natarajan K, Mori N, Artemov D, Bhujwalla ZM. Exposure of human breast cancer cells to the anti-inflammatory agent indomethacin alters choline phospholipid metabolites and Nm23 expression. Neoplasia 2002;4:409–16.
12. Glunde K, Ackerstaff E, Natarajan K, Artemov D, Bhujwalla ZM. Real-time changes in 1H and 31P NMR spectra of malignant human mammary epithelial cells during treatment with the anti-inflammatory agent indomethacin. Magn Reson Med 2002; 48:819–25.
13. Mori N, Natarajan K, Chacko VP, Artemov D, Bhujwalla ZM. Choline phospholipid metabolites of human vascular endothelial cells altered by cyclooxygenase inhibition, growth factor depletion, and paracrine factors secreted by cancer cells. Mol Imaging 2003;2:124–30.
14. Inglese M, Li BS, Rusinek H, Babb JS, Grossman RI, Gonen O. Diffusely elevated cerebral choline and creatine in relapsing-remitting multiple sclerosis. Magn Reson Med 2003;50:190–5.
15. Pettegrew JW, Klunk WE, Panchalingam K, McClure RJ, Stanley JA. Magnetic resonance spectroscopic changes in Alzheimer's disease. Ann N Y Acad Sci 1997; 826:282–306.
16. Bodennec J, Pelled D, Riebeling C, Trajkovic S, Futerman AH. Phosphatidylcholine synthesis is elevated in neuronal models of Gaucher disease due to direct activation of CTP:phosphocholine cytidylyltransferase by glucosylceramide. FASEB J 2002;16: 1814–6.
17. Lutz NW, Tome ME, Cozzone PJ. Early changes in glucose and phospholipid metabolism following apoptosis induction by IFN-gamma/TNF-alpha in HT-29 cells. FEBS Lett 2003;544:123–8.
18. Ronen SM, Degani H. The application of 13C NMR to the characterization of phospholipid metabolism in cells. Magn Reson Med 1992;25:384–9.
19. Katz-Brull R, Seger D, Rivenson-Segal D, Rushkin E, Degani H. Metabolic markers of breast cancer: enhanced choline metabolism and reduced choline-ether-phospholipid synthesis. Cancer Res 2002;62:1966–70.
20. Paine TM, Soule HD, Pauley RJ, Dawson PJ. Characterization of epithelial phenotypes in mortal and immortal human breast cells. Int J Cancer 1992;50:463–73.
21. Tyagi RK, Azrad A, Degani H, Salomon Y. Simultaneous extraction of cellular lipids and water-soluble metabolites: evaluation by NMR spectroscopy. Magn Reson Med 1996;35:194–200.
22. Li C, Wong WH. Model-based analysis of oligonucleotide arrays: expression index computation and outlier detection. Proc Natl Acad Sci USA 2001;98:31–6.
23. Li C, Hung Wong W. Model-based analysis of oligonucleotide arrays: model validation, design issues and standard error application. Genome Biol 2001;2:research0032.0031–0032.0011.
24. Katz-Brull R, Degani H. Kinetics of choline transport and phosphorylation in human breast cancer cells; NMR application of the zero trans method. Anticancer Res 1996;16:1375–80.
25. Ramirez de Molina A, Gutierrez R, Ramos MA, et al. Increased choline kinase activity in human breast carcinomas: clinical evidence for a potential novel antitumor strategy. Oncogene 2002;21:4317–22.
26. Noh DY, Ahn SJ, Lee RA, et al. Overexpression of phospholipase D1 in human breast cancer tissues. Cancer Lett 2000;161:207–14.
27. Zhong M, Shen Y, Zheng Y, Joseph T, Jackson D, Foster DA. Phospholipase D prevents apoptosis in v-Src-transformed rat fibroblasts and MDA-MB-231 breast cancer cells. Biochem Biophys Res Commun 2003;302:615–9.
28. Yamashita S, Yamashita J, Ogawa M. Overexpression of group II phospholipase A2 in human breast cancer tissues is closely associated with their malignant potency. Br J Cancer 1994;69:1166–70.
29. Guthridge CJ, Stampfer MR, Clark MA, Steiner MR. Phospholipases A2 in ras-transformed and immortalized human mammary epithelial cells. Cancer Lett 1994; 86:11–21.
30. Bolan PJ, DelaBarre L, Baker EH, et al. Eliminating spurious lipid sidebands in 1H MRS of breast lesions. Magn Reson Med 2002;48:215–22.
31. Cheng LL, Chang IW, Smith BL, Gonzalez RG. Evaluating human breast ductal carcinomas with high-resolution magic-angle spinning proton magnetic resonance spectroscopy. J Magn Reson 1998;135:194–202.
32. Rodriguez-Gonzalez A, de Molina AR, Fernandez F, et al. Inhibition of choline kinase as a specific cytotoxic strategy in oncogene-transformed cells. Oncogene 2003;22:8803–12.